Organic Electronics 14 (2013) 1931–1938

Contents lists available at SciVerse ScienceDirect

Organic Electronics

journal homepage: www.elsevier.com/locate/orgel

Enhanced carrier mobility and photon-harvesting property by introducing Au nano-particles in bulk heterojunction photovoltaic cells

Soo Won Heo [a], Eui Jin Lee [a], Kwan Wook Song [a], Jang Yong Lee [b], Doo Kyung Moon [a,*]

[a] Department of Materials Chemistry and Engineering, Konkuk University, 1 Hwayang-dong, Gwangjin-gu, Seoul 143-701, Republic of Korea
[b] Energy Materials Research Center, Korea Research Institute of Chemical Technology, P.O. Box 107, Yuseong, Daejeon 305-600, Republic of Korea

ARTICLE INFO

Article history:
Received 23 August 2012
Received in revised form 21 April 2013
Accepted 21 April 2013
Available online 9 May 2013

Keywords:
Polymer solar cells (PSCs)
Photon-harvesting property
Au nanoparticles (NPs)
Carrier mobility
Localized surface plasmon resonance (LSPR)

ABSTRACT

In this study, polymer solar cells (PSCs) doped with Au nanoparticles (Au NPs) were successfully fabricated to maximize the photon-harvesting properties on the photoactive layer. In addition, a conductivity-enhanced hybrid buffer layer was introduced to improve the photon absorption properties and effectively separate the generated charges by adding Au NPs and dimethylsulfoxide (DMSO) to the PH 500 as a buffer layer. The PSC performance was optimized with a 88% improvement over the conventional PSCs (photoactive area: 225 mm^2, power conversion efficiency (PCE): 3.2%) by the introduction to the buffer layer of Au NPs and DMSO at 10 wt% and 1.0 wt%, respectively, and with 15 wt% Au NP doping in the photoactive layer. The internal resistance was decreased due to the increased photocurrent caused by the localized surface plasmon resonance (LSPR) effect of the Au NPs in the photoactive layer and by the improvement of carrier mobility induced by the DMSO doping of the buffer layer. As a result, the series resistance (R_S) deceased from 42.3 to 19.7 $\Omega\,cm^2$ while the shunt resistance (R_{SH}) increased from 339 to 487 $\Omega\,cm^2$.

1. Introduction

The π-conjugated polymer-based polymer solar cells (PSCs) have the advantage of easy fabrication of lightweight devices with superior mechanical properties. Therefore, if spin-coating, ink-jet printing, roll-to-roll printing, brush painting or stamping techniques are applied to the flexible substrate, lightweight and flexible, large-area photovoltaic devices can be fabricated at low cost. [1–7]. At present, the power conversion efficiency (PCE) of the PSCs with a photoactive area (or aperture area) of ca. $1cm^2$ or smaller is 8–10%, which is too low to fabricate a large-area cell or module [8,9]. For PCE improvement, it is necessary to increase the open circuit voltage (V_{OC}) and short circuit current density (J_{SC}) [10]. V_{OC} is dependent on the difference between the highest occupied molecular orbital (HOMO) level of the polymer and the lowest unoccupied molecular orbital level of fullerene in the polymer-fullerene-based bulk heterojunction system [11]. Therefore, V_{OC} can be enhanced through the molecular structure design in polymer materials, whereas J_{SC} can be increased by modifying the device geometries. Some studies have reported that the photon absorption properties were enhanced by introducing a titanium suboxide film for an optical spacer layer [12], or J_{SC} was improved by reducing the leakage current after adopting a nickel oxide film as the electron-blocking layer [13]. In addition, J_{SC} can be increased by improving the carrier mobility after adopting water/alcohol soluble polymer films as the hole or electron-collecting layer [14] or improving the polymer ordering by adding processing additives to the photoactive layer [15]. However, J_{SC} is most influenced by the photon-harvesting properties on the photoactive layer [16]. Therefore, it can be increased after enhancing the photon-harvesting properties on the photoactive layer and separating the photogenerated carrier into

* Corresponding author. Tel.: +82 2 450 3498; fax: +82 2 444 0765.
E-mail address: dkmoon@konkuk.ac.kr (D.K. Moon).

1566-1199/$ - see front matter © 2013 Elsevier B.V. All rights reserved.
http://dx.doi.org/10.1016/j.orgel.2013.04.042

the external circuit quickly before they are recombined, as we have previously reported [17].

One of the key issues in achieving high performance is gaining sufficient photon absorption of the photoactive layer, i.e., efficient harvesting of sunlight. Nevertheless, the use of a thicker active layer inevitably increases the device resistance because of the low carrier mobilities of organic materials. As a result, we previously found that the efficiency is decreased [17]. In terms of enhancing the light absorption without having to change the film thickness, therefore, we have previously investigated the exploitation of localized surface plasmon resonance (LSPR) [17,18]. The excitation of LSPR through the resonant interaction between the electromagnetic field of incident light and the surface electron density surrounding metallic nanoparticles (NPs) causes local enhancement in the electromagnetic field, which is expected to enhance light harvesting in the PSCs [19,20]. To increase the PCE, therefore, many groups were introduced Au NPs in either the buffer layer or the photoactive layer [16,21]. In addition, Xie et al. introduced Au NPs in the buffer layer and the photoactive layer [22]. As a result, numerous holes and electrons could be effectively generated because of the LSPR-induced improvement in the photon-harvesting properties.

However, the problem of recombination has arisen because the separated holes and electrons failed to exit to the external circuit due to the low conductivity of the polymer or buffer layer. To solve this problem, we previously enhanced both J_{SC} and the fill factor (FF) by reducing the series resistance (R_S) after introducing a conductivity-enhanced buffer layer (photoactive area: 225 mm^2) [17].

In this study, therefore, to maximize the absorption of photons, Au NPs were introduced to both the buffer layer and the photoactive layer. To effectively separate the generated charges and prevent recombination before exiting to the external circuit, in addition, dimethylsulfoxide (DMSO) was added to the buffer layer. Consequently, the properties were optimized with a PCE of 3.2% (photoactive area: 225 mm^2) in a device in which 10 wt% of Au NPs and 1 wt% of DMSO were added to the buffer layer and 15 wt% of Au NPs was added to the photoactive layer. To investigate this improvement in the PSC properties, the optical and electrical properties of the buffer and photoactive layers to which metal NPs had been introduced were observed.

In addition, the photon absorption and the quenching properties of the excited electrons were observed through ultraviolet/photoluminescence (UV/PL) spectroscopy. The images and surface morphology of the Au NPs distributed in each layer were observed through scanning electron microscopy (SEM) and atomic force microscopy (AFM) analysis. In addition, the dependence of the carrier mobilities on the presence and absence of Au NPs was measured using the space charge limited current (SCLC) method.

2. Materials and measurements

2.1. Materials

Conventional PEDOT:PSS (AI 4083) and modified PEDOT:PSS (PH 500) were purchased from Clevios. DMSO, which was used to enhance the conductivity of PH500, was purchased from Aldrich. P3HT, a donor material in the photoactive layer, was purchased from Rieke Metals, while the acceptor material PCBM was bought from Nano C (Fig. 1). Octahedral and truncated octahedral-structured Au NPs were synthesized in accordance with the method mentioned in the literature [23,24].

2.2. Measurements

All thin films were fabricated using a GMC2 spin coater (Gensys), and the thickness was measured with an alpha step 500 surface profiler (KLA-Tencor). The surface plasmon resonance (SPR) absorption band and nanocrystal images were measured with UV–vis spectroscopy (HP Agilent 8453) and field effect SEM (FE-SEM, JEOL JSM-6701F), respectively, by determining the size of the synthesized Au NPs. X-ray diffraction (XRD) patterns were observed using a Rigaku D/MAX 2200 diffractometer with Cu Kα radiation. The electrical properties of the hybrid buffer layer were measured using a 4-point probe station (MST6000C). The surface of the fabricated device was observed through AFM (PSIA XE-100) and FE-SEM. The *J–V* characteristics of the PSCs were measured using a Keithley 2400 source measure unit. The devices were evaluated at 298 K by using a Class A Oriel solar simulator (Oriel 96000 150 W solar simulator) with a xenon lamp that simulates AM 1.5G irradiation (100 mW/cm^2) from 400 to 1100 nm. The instrument was calibrated with a monocrystalline Si diode fitted with a KG5 filter to bring the spectral mismatch to unity. The calibration standard was calibrated by the National Renewable Energy Laboratory (NREL). IPCE (Mc science) was measured against the best performance device.

3. Experimental part

3.1. Cleaning of ITO glass and bare glass

To clean the ITO glass (10 Ω/sq, Samsung corning) and bare glass, detergent (Alconox® in deionized water, 10%), acetone, isopropyl alcohol and deionized water were each sonicated in order for 20 min. The moisture was removed by blowing thoroughly with N_2 gas. To ensure complete removal of all of the remaining water, the ITO glass and bare

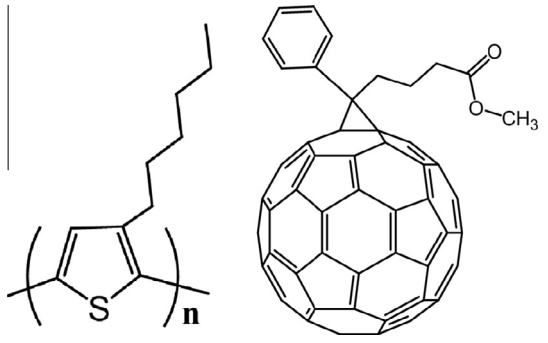

Fig. 1. Molecular structures of photovoltaic materials (donor: P3HT, acceptor: $PC_{61}BM$).

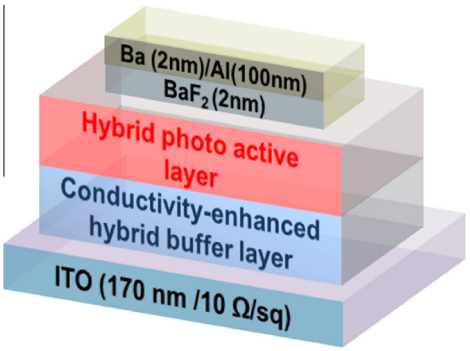

Fig. 2. Schematic of photovoltaic device.

glass were baked on a hot plate for 10 min at 100 °C. For hydrophilic treatment of the ITO glass and bare glass surface, they were cleaned for 10 min in a UVO cleaner.

3.2. Synthesis of Au NPs

The Au NPs used in this study were synthesized according to the literature method [23,24]. During the synthesis, the SPR absorption band according to the particle size was measured through UV–vis spectroscopy. In addition, the size and shape of the Au NPs were observed through FE-SEM, and the crystal structure of the Au NPs was analyzed through the XRD patterns.

3.3. Formulation of buffer layer ink and fabrication of buffer layers

To measure the electrical properties of modified PEDOT:PSS (PH 500), they were spin-coated at 4000 rpm on a cleaned bare glass and annealed at 120 °C for 20 min. The electrical properties of the thin films thus fabricated were measured using a 4-point probe station. To measure the electrical properties of PH500 according to the octahedral-structured Au NP doping concentration, Au NPs solution (0.1 mg/ml) (ca. 30 nm size) was doped at 5, 10 and 15 wt%. Then, a hybrid buffer layer ink was formulated and its conductivity was increased by doping with DMSO at 0.5, 1.0 and 2.0 wt%. To observe the electrical properties, surface morphology and distribution of the Au NPs of the resulting conductivity-enhanced hybrid buffer layer, the solutions were spin-coated at 4000 rpm in a cleaned bare glass and annealed at 120 °C for 20 min. The characteristics of the fabricated thin films were measured through a 4-point probe station and AFM.

3.4. Fabrication of PSCs

3.4.1. Optimization of the Au NP doping concentration

To effectively harvest photons through LSPR, the concentration of the Au NPs that were doped in the buffer and photoactive layers was optimized. As shown in Fig. 2, PSCs with a conductivity-enhanced hybrid buffer layer and a hybrid photoactive layer were fabricated. After spin-coating PH500 in which octahedral-structured Au NPs were doped on the patterned ITO glass at 5, 10 and 15 wt%, a 40-nm-thick hybrid buffer layer was formed. Then, solutions were annealed on the hot plate at 120 °C for 20 min to remove any residual solvents. The solutions that had been blended with an ortho-dichlorobenzene (ODCB) concentration of 1.5 wt% and a P3HT/PCBM ratio of 1:0.6, and had been doped with truncate octahedral-structured Au NPs at 10, 15 and 20 wt% for a photoactive layer were spin-coated at 500 rpm on the hybrid buffer layer to form a 130-nm-thick layer and then annealed at 160 °C for 10 min. To form the cathode, BaF_2 (0.1 Å/s, 2 nm), Ba (0.2 Å/s, 2 nm) and Al (5 Å/s, 100 nm) were thermally deposited in order in a high-vacuum chamber. Finally, large-area PSCs with an active area of 225 mm^2 (15 mm × 15 mm) were fabricated through encapsulation.

4. Results and discussion

Fig. 3 shows the SEM images of the synthesized Au NPs. As shown in Fig. 3a, the Au NPs applied to the buffer layer were octahedral-structured with a particle size of ca. 30 nm. In our previous study, we reported that it was possible to adjust the particle size by adjusting response time during the Au NP synthesis [17]. In this study, therefore, Au NPs sized ca. 30 nm were introduced by reducing the Au NP synthesis time for embedment into the buffer layer (ca. 40 nm in thickness). The strong intensity of the (1 1 1) reflection peak indicated that the octahedra were bounded by {1 1 1} faces and that they were deposited preferentially with their triangular faces on the substrate surface. Fig. 3b shows an SEM image of the truncated octahedral-structured Au NPs sized ca. 80 nm that were applied into the photoactive layer. The photo absorption properties of the Au NPs were more dependent on the particle size than on the shape [25,26]. Therefore, the particle size was controlled using a different synthesis method from that applied to the buffer layer [27]. Fig. 4 shows the SPR absorption band according to the particle size and shape of the Au NPs. In terms of maximum absorption peak (λ_{max}), the octahedral-structured Au NPs (ca. 80 nm size) were 568 nm while the truncated octahedral-structured Au NPs of the same size were 571 nm. However, the octahedral-structured Au NPs sized ca. 30 nm were 550 nm, and were blue shifted by approximately 18 nm. Therefore, this result confirmed that the absorbance property of the Au NPs was more dependent on the particle size than on the shape.

Table 1 summarizes the electrical properties of the buffer layer according to the doping concentration of the Au NPs and DMSO. When Au NPs was doped at 10 wt%, the conductivity was 0.21 S/cm, which was improved by about 40% compared to the undoped layer. When the doping concentration of Au NPs was 15 wt%, however, the PEDOT and PSS agglomeration dramatically increased. As a result, the root mean square (RMS) value increased from 3.21 to 4.52 nm, which in turn decreased the conductivity. In addition, the DMSO doping level was optimized to enhance the conductivity of the Au NPs-doped hybrid buffer layer, and the electrical properties are summarized in Table 1. The polar solvents with high dielectric constant such as DMSO, increased the conductivity of PEDOT:PSS by reducing the

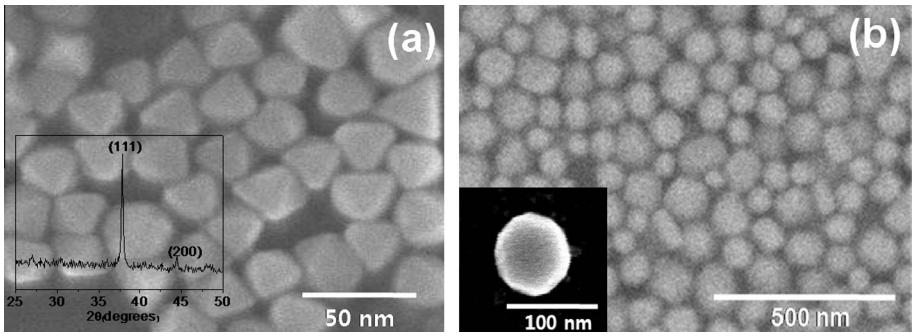

Fig. 3. (a) SEM image of octahedral Au NPs (inset shows XRD pattern of octahedral Au NPs). (b) SEM image of truncated octahedral Au NPs (Inset shows the truncated octahedral Au nanoparticle in greater detail).

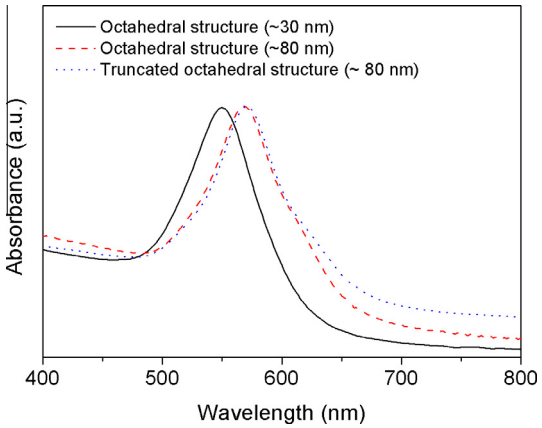

Fig. 4. Surface plasmon resonance (SPR) absorption bandof Au NPs.

coulombic interaction between the counter ion and the charge carrier through the strong positively charged PEDOT-negatively charged PSS dopant screen effects [28,29]. Therefore, as the DMSO doping level was increased, the conductivity of the hybrid buffer layer increased. The highest conductivity was observed at 2 wt% doping. Even though the doping concentration of the Au NPs was fixed, however, the degree of PEDOT/PSS agglomeration, which was similar to Au NPs in terms of size, increased when the DMSO doping level increased, which in turn degraded the morphology of the thin film. Consequently, the highest conductivity was detected at the thin film in which DMSO and Au NPs were doped at 2.0 wt% and by 10 wt%, respectively, to PH500. The conductivity was 139 S/cm.

To confirm the improvement of photovoltaic properties after the introduction of the photoactive layer that had been doped with the conductivity-enhanced hybrid buffer layer and Au NPs and the optimized production conditions, PSCs were fabricated. After spin-coating various types of buffer layer inks that were formulated on the patterned ITO glass, a thickness of 40 nm was obtained. The layers were then annealed at 120 °C for 20 min. As photoactive layers, P3HT and PCBM were mixed at 1:0.6 ratio and blended in ODCB in 1.5 wt% concentration. Then, the solutions in which Au NPs had been doped at 10, 15 and 20 wt% were spin-coated on the buffer layer to give a thickness of about 130 nm. The layer was then annealed at 160 °C for 10 min. To form the cathode, thermal deposition was carried out in a high vacuum chamber in the order of BaF_2 (0.1 Å/s, 2 nm), Ba (0.2 Å/s, 2 nm) and Al (5 Å/s, 100 nm). Because organic materials and metals differ from each other in terms of surface energy and energy level, BaF_2 was applied as an electron transporting layer for effective collection of electrons through ohmic contact. In addition, Ba (−2.7 eV) with low work function was used as the cathode, and Al was deposited to a thickness of 10 nm to protect the cathode.

Fig. 5 shows the characteristics of the PSCs and incident photon to current efficiency (IPCE) data, and the details are presented in Table 2. In the case of the pristine

Table 1
Electrical properties of hybrid buffer layers and conductivity-enhanced hybrid buffer layers at various concentrations of Au NPs and DMSO.

	Hybrid buffer layers				Conductivity enhanced hybrid buffer layers											
Additives concentrations (wt%)	–				0.5				1.0				2.0			
Au NPs concentrations[a] (wt%)	0	5	10	15	0	5	10	15	0	5	10	15	0	5	10	15
Resistivity (Ω cm)	6.32	5.82	4.75	5.72	0.232	0.195	0.120	0.184	0.065	0.057	0.049	0.053	0.009	0.008	0.007	0.008
Conductivity (S/cm)	0.15	0.17	0.21	0.17	4.31	5.13	8.32	5.43	15.4	17.5	20	18.9	105	114	139	117
Root mean square[b] roughness (nm)	3.21	3.42	3.78	4.52	4.13	5.24	6.47	7.21	5.32	6.54	7.59	8.17	6.27	7.59	8.26	9.14

[a] Au NPs crystalline size: ~30 nm, Au NPs solution: 0.1 mg/ml. Buffer layer thickness: 40 nm, Annealing: 20 min at 120 °C.
[b] Root mean square roughness values were measured by atomic force microscopy.

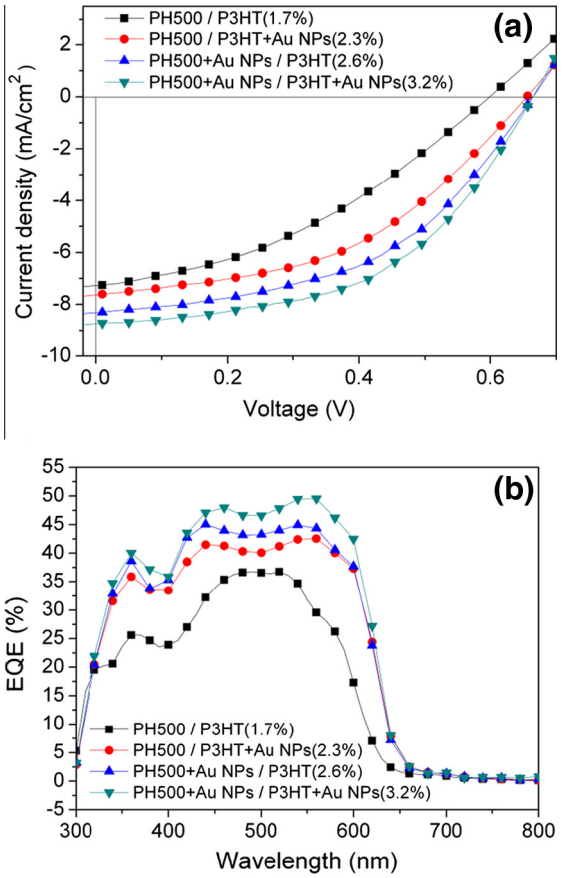

Fig. 5. (a) *J–V* characteristics of the PSCs for various modified buffer layers and photo active layers. (b) IPCE data of fabricated devices for various modified buffer layers and photo active layers.

PH500-applied reference device, J_{SC}, V_{OC} and FF were 7.3 mA/cm^2, 0.595 V and 37.8%, respectively. The calculated PCE was 1.7%. To increase the photon absorption in the photoactive layer, truncated octahedral-structured Au NPs were doped at various concentrations. The PSC performance was optimized at Au NP dopant concentration of 15 wt%, and PCE was improved by about 35–2.3%, compared to the reference device. The Au NP doping increased the shunt resistance (R_{SH}) from 339 to 384 Ω cm^2 and J_{SC} from 7.3 to 7.6 mA/cm^2. When R_S decreased from 42.3 to 32.9 Ω cm^2, the leakage current also decreased. As a result, FF increased by about 28%. In particular, V_{OC} significantly improved from 0.595 to 0.656 V. According to the report of the Heeger group, the P3HT:PCBM based BHJ layer with Au NPs have a work function of approximately 5.1 eV (close to the highest occupied molecular orbital (HOMO) energy level of P3HT, 5.2 eV), thus resulting in a small energy barrier for hole extraction. Therefore, the introduction of Au NPs decreases hole injection barrier to 0.1 eV. This smaller hole injection barrier can induce a cascade hole transfer from the HOMO energy of P3HT to the ITO electrode. Efficient hole extraction can reduce the possibility of electron / hole recombination, thus resulting in the increase of V_{OC} [24].

To improve the photon absorption property and carrier mobility on the buffer layer, octahedral-structured Au NPs and DMSO were introduced to the PH500. The device performance was optimized at Au NPs and DMSO dopant levels of 10 wt% and 1 wt%, respectively. In addition, PCE improved by about 53–2.6%, compared to the reference device. In particular, R_S (25.3 Ω cm^2) decreased by about 60% while R_{SH} (430 Ω cm^2) increased by 27%, compared to the reference device, because of the improved conductivity of the buffer layer by adding DMSO to the hybrid buffer layer. We previously ascertained that these resistance changes decreased the probability of recombination due to the fast shift of the holes and electrons generated in the photoactive layer to the external circuit [17]. Therefore, it was confirmed that J_{SC} increased from 7.3 to 8.3 mA/cm^2 and FF from 37.8% to 48.6%.

The PCE of the PSCs in which the photoactive layer had been doped with conductivity-enhanced hybrid buffer layer and Au NPs was 3.2%, which was an increase of 88% compared to the reference device. J_{SC}, FF and V_{OC} increased from 7.3 to 8.7 mA/cm^2, 37.8% to 56.1% and 0.595 to 0.656 V, respectively. Because of the increase of photocurrent by the LSPR effect of the Au NPs on the photoactive layer and the improvement of the carrier mobility by the DMSO-doped buffer layer, the internal resistance decreased, and R_S decreased from 42.3 to 19.7 Ω cm^2. In particular, R_{SH} increased from 339 to 487 Ω cm^2. This confirmed the decreased charge recombination at a photoactive layer and buffer layer interface. Therefore, FF increased by over 48%, which improved the photon-harvesting properties on both the buffer and photoactive layers by applying both the conductivity-enhanced hybrid buffer layer and the Au NPs-doped photoactive layer. In addition, the probability of charge recombination was simply reduced by improving the carrier mobility via the enhanced conductivity of the buffer layer.

Fig. 5b shows the IPCE data of the PSCs. Compared to the devices which were not doped with Au NPs, the increased external quantum efficiency (EQE) occurred mostly in the Au NPs-doped devices. In particular, the

Table 2
Characteristics of devices.

	J_{SC} (mA/cm^2)	V_{OC} (V)	FF (%)	PCE (%)	R_s (Ω cm^2)	R_{sh} (Ω cm^2)
PH500/P3HT	7.3	0.595	37.8	1.7	42.3	339
PH500/P3HT + Au NPs 15 wt%	7.6	0.656	45.2	2.3	32.9	384
PH500 + DMSO 1 wt% + Au NPs 10%/P3HT	8.3	0.656	48.6	2.6	25.3	430
PH500 + DMSO 1 wt% + Au NPs 10%/P3HT + Au NPs 15 wt%	8.7	0.656	56.1	3.2	19.7	487

ITO/PH500 w/w.o Au NPs and DMSO/P3HT:PCBM(1:0.6) w/w.o Au NPs/BaF_2/Ba/Al.

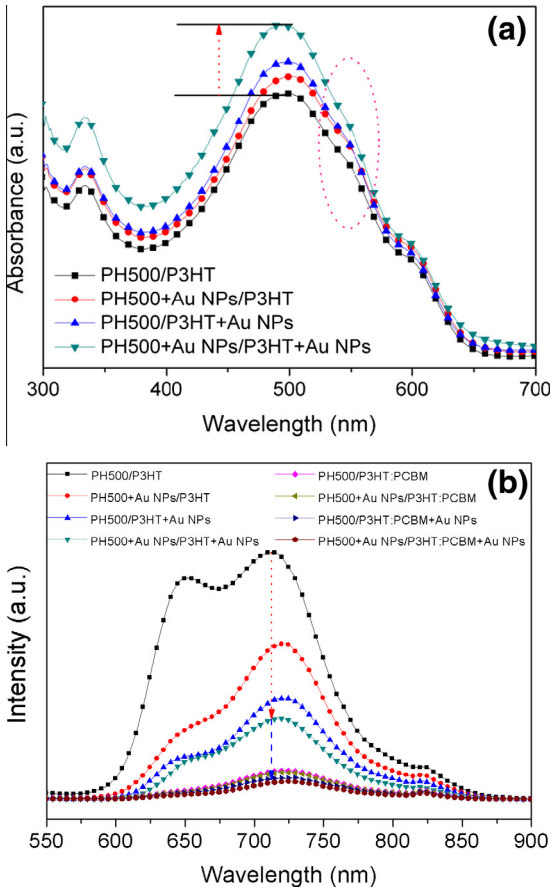

Fig. 6. (a) Photon absorption property of various modified buffer layers and photo active layers (b).

maximum EQE was 37% at ca. 520 nm in the devices without Au NPs and 50% at ca. 550–570 nm region in the Au NPs-doped devices. The same result was also found within the photon absorption range of the Au NPs (ca. 550–570 nm), which confirmed the increase in the photon-harvesting properties by the LSPR effect after the introduction of the Au NPs.

To determine if the holes and electrons that were dissociated with the photon-harvesting properties because of the application position of Au NPs were effectively shifted to the external circuit, the UV–vis absorption data and PL quenching data were analyzed. According to Fig. 6a, in the case of photo active layer with Au NPs, the absorption property was more increased than that of buffer layer with Au NPs. LSPR of Au NPs are very sensitive to the sizes, shapes as well as the surrounding environment [17]. Therefore, the difference in absorbance is due to the difference in the size and the shape of the Au NPs. The photon absorption properties were more improved in the sample in which Au NPs were introduced to both buffer and photoactive layers than in the sample without Au NPs. In particular, the absorption properties were dramatically increased in a range of below 560 nm, because the scattered photons form buffer layer was absorbed in photoactive layer. Therefore, we successfully introduced Au NPs in both layers to enhance the absorption over a larger wavelength region (see Table 3).

Fig. 6b presents the PL quenching data. The difference between the area without PCBM (acceptor) and the PCBM-included area represents the quenched electron holes. With increasing quenched amount, the electron holes were dissociated more efficiently. The Au NP doping quenched the photons even in the absence of the PCBM acceptor. This result confirmed that the Au NPs absorbed the photons well because of the LSPR effect. The quenching properties were improved when doped with the photoactive layer instead of with the buffer layer. In addition, they were improved the most when they were added to both layers. The quenching rate was 89% when PCBM (acceptor) was added without any Au NP doping. When Au NPs were doped in both buffer and photoactive layers, on the contrary, the quenching rate reached up to 95%. Therefore, Au NP doping enhanced the photon absorption properties in the photoactive and buffer layers through the LSPR effect. The improved conductivity of the buffer layer achieved by DMSO addition enhanced the PCE of the PSCs by letting the absorbed photons exit to the external circuit before being recombined.

After fabricating a hole-only device for a charge mobility study, the hole mobilities were calculated using the SCLC [30–32]. The configuration of hole-only devices and the graphs of the logarithm of JL^3/V^2 versus the square root of the mean electric field are shown in Fig. 7. The device with conventional PEDOT:PSS exhibited a hole mobility of 3.80×10^{-2} cm^2/Vs, compared to 2.83 cm^2/Vs for the device which used pristine PH500. In addition, the device in which Au NPs were doped to the photoactive layer had a hole mobility of 3.13 cm^2/Vs, which indicated that Au NPs improved carrier mobility. However, the hole mobility was higher in the device which enhanced the conductivity of the buffer layer to 4.22 cm^2/Vs. When Au NPs were doped in both layers, the hole mobility improved up to 5.99 cm^2/Vs. This result confirmed that Au NP doping improved the photon-harvesting properties in both the photoactive and buffer layers and also enhanced the hole mobility. Further-

Table 3
PL quenching rate of various structures of buffer layer and photo active layer.

	Quenching rate (%)
PH500/P3HT	89
PH500/P3HT + Au NPs 15 wt%	92
PH500 + DMSO 1 wt% + Au NPs 10%/P3HT	91
PH500 + DMSO 1 wt% + Au NPs 10%/P3HT + Au NPs 15 wt%	94

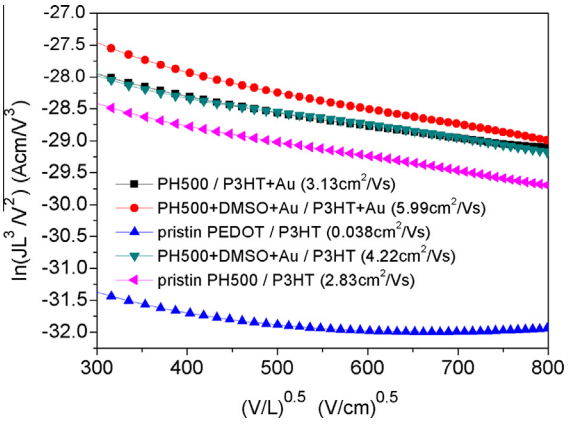

Fig. 7. Current (J)–voltage (V) characteristics of the hole-only devices with pristine PEDOT:PSS/P3HT, pristine PH 500/P3HT, PH 500/P3HT + Au NPs, PH 500 + DMSO + Au NPs/P3HT and PH 500 + DMSO + Au NPs/P3HT + Au NPs measured in the dark.

more, DMSO was able to send the generated holes to the external circuit quickly without recombination after the conductivity of the buffer layer was improved.

5. Conclusion

In this study, a conductivity-enhanced hybrid buffer layer was introduced to PSCs to improve their photon-harvesting properties based on the LSPR effect, by adding octahedral-structured Au NPs, and effectively separate the generated charges, by adding DMSO to PH 500 as a buffer layer. In addition, PSCs doped with truncated octahedral-structured Au NPs were successfully fabricated to maximize the photon-harvesting properties on the photoactive layer. The addition of Au NPs and DMSO to the buffer layer at 10 wt% and 1.0 wt%, respectively, and of Au NPs to the photoactive layer at 15 wt%, led to the optimization of the PSC characteristics with a PCE of 3.2%. The internal resistance was decreased due to the increase in the photocurrent induced by the LSPR effect of the Au NPs that had been introduced to the photoactive layer and the improvement of carrier mobility by the DMSO-doped buffer layer. As a result, R_S decreased from 42.3 to 19.7 $\Omega\,cm^2$, while R_{SH} increased from 339 to 487 $\Omega\,cm^2$, which confirmed the decrease in the charge recombination in the buffer and photoactive layer interface. Therefore, the introduction of both the conductivity-enhanced hybrid buffer layer and the Au NP-doped photoactive layer enhanced the photon-harvesting properties on both the buffer and the photoactive layers. In this simple method, the probability of charge recombination was reduced by enhancing the carrier mobility after improving the conductivity of the buffer layer.

Acknowledgement

This research was supported by a Grant (10037195) from the Fundamental R&D Program for Core Technology of Materials funded by the Ministry of Knowledge Economy and supported from the technology supporting Project Grant funded by the Korea government Ministry of Knowledge Economy (No. 2012K10042360)

References

[1] F.C. Krebs, J. Fyenbob, M. Jørgensen, Product integration of compact roll-to-roll processed polymer solar cell modules: methods and manufacture using flexographic printing, slot-die coating and rotary screen printing, J. Mater. Chem. 20 (2010) 8994.
[2] F.C. Krebs, Fabrication and processing of polymer solar cells: a review of printing and coating techniques, Sol. Energy Mater. Sol. Cells 93 (2009) 394.
[3] J. Alstrup, M. Jørgensen, A.J. Medford, F.C. Krebs, Ultra fast and parsimonious materials screening for polymer solar cells using differentially pumped slot-die coating, ACS Appl. Mater. Interfaces 2 (2010) 2819.
[4] E. Bundgaard, O. Hagemann, M. Manceau, M. Jørgensen, F.C. Krebs, Low band gap polymers for roll-to-roll coated polymer solar cells, Macromolecules 43 (2010) 8115.
[5] F.C. Krebs, T.D. Nielsen, J. Fyenbo, M. Wadstrøm, M.S. Pedersen, Manufacture, integration and demonstration of polymer solar cells in a lamp for the "Lighting Africa" initiative, Energy Environ. Sci. 3 (2010) 512.
[6] S.W. Heo, J.Y. Lee, H.J. Song, J.R. Ku, D.K. Moon, Patternable brush painting process for fabrication of flexible polymer solar cells, Sol. Energy Mater. Sol. Cells 95 (2011) 3041.
[7] S.W. Heo, K.W. Song, M.H. Choi, T.H. Sung, D.K. Moon, Patternable solution process for fabrication of flexible polymer solar cells using PDMS, Sol. Energy Mater. Sol. Cells 95 (2011) 3564.
[8] L. Dou, J. You, J. Yang, C.-C. Chen, Y. He, S. Murase, T. Moriarty, K. Emery, G. Li, Y. Yang, Tandem polymer solar cells featuring a spectrally matched low-bandgap polymer, Nat. Photonics 6 (2012) 180;
Z. He, C. Zhong, S. Su, M. Xu, H. Wu, Y. Cao, Nat. Photonics 6 (2012) 591;
X. Li, W.C.H. Choy, L. Huo, F. Xie, W.E.I. Sha, B. Ding, X. Guo, Y. Li, J. Hou, J. You, Y. Yang, Dual plasmonic nanostructures for high performance inverted organic solar cells, Adv. Mater. 24 (2012) 3046.
[9] Web references, Last access on September 27, 2012. (a) <http://www.mitsubishichem-hd.co.jp/english/group/strategy/major_project/solar_cell.html>. (b) <http://www.polyera.com/newsflash/polyera-achieves-world-record-organic-solar-cell-performance>.
[10] A.K. Pandey, M. Aljada, M. Velusamy, P.L. Burn, P. Meredith, Nanostructured, active organic–metal junctions for highly efficient charge generation and extraction in polymer-fullerene solar cells, Adv. Mater. 24 (2012) 1055.
[11] J.Y. Lee, W.S. Shin, J.R. Haw, D.K. Moon, Low band-gap polymers based on quinoxaline derivatives and fused thiophene as donor materials for high efficiency bulk-heterojunction photovoltaic cells, J. Mater. Chem. 19 (2009) 4938.
[12] J.Y. Kim, S.H. Kim, H. Lee, K. Lee, W. Ma, X. Gong, A.J. Heeger, New architecture for high-efficiency polymer photovoltaic cells using solution-based titanium oxide as an optical spacer, Adv. Mater. 18 (2006) 572.
[13] M.D. Irwin, D.B. Buchholz, A.W. Hains, R.P.H. Chang, T.J. Marks, p-Type semiconducting nickel oxide as an efficiency-enhancing anode interfacial layer in polymer bulk-heterojunction solar cells, Proc. Nat. Acad. Sci. USA 105 (2008) 2783.
[14] Z. He, C. Zhang, X. Xu, L. Zhang, L. Huang, J. Chen, H. Wu, Y. Cao, Largely enhanced efficiency with a PFN/Al bilayer cathode in high efficiency bulk heterojunction photovoltaic cells with a low bandgap polycarbazole donor, Adv. Mater. 23 (2011) 3086.
[15] Y. Yao, J. Hou, Z. Xu, G. Li, Y. Yang, Effects of solvent mixtures on the nanoscale phase separation in polymer solar cells, Adv. Funct. Mater. 18 (2008) 1783.
[16] (a) F.C. Chen, J.L. Wu, C.L. Lee, Y. Hong, C.H. Kuo, M.H. Huang, Plasmonic-enhanced polymer photovoltaic devices incorporating solution-processable metal nanoparticles, Appl. Phys. Lett. 95 (2009) 013305;
(b) D.D.S. Fung, L. Qiao, W.C.H. Choy, C. Wang, W.E.I. Sha, F. Xie, S. He, Optical and electrical properties of efficiency enhanced polymer solar cells with Au nanoparticles in a PEDOT:PSS layer, J. Mater. Chem. 21 (2011) 16349.
[17] S.W. Heo, I.S. Song, Y.S. Kim, D.K. Moon, Fabrication of OPVs by introducing a conductivity-enhanced hybrid buffer layer, Sol. Energy Mater. Sol. Cells 101 (2012) 295.

[18] J.H. Lee, J.H. Park, J.S. Kim, D.Y. Lee, K. Cho, High efficiency polymer solar cells with wet deposited plasmonic gold nanodots, Org. Electron. 10 (2009) 416.
[19] S. Lal, S. Link, N.J. Halas, Nano-optics from sensing to waveguiding, Nature Photon. 1 (2007) 641.
[20] E. Hutter, J.H. Fendler, Exploitation of localized surface plasmon resonance, Adv. Mater. 16 (2004) 1685.
[21] C.C.D. Wang, W.C.H. Choy, C. Duan, D.D.S. Fung, W.E.I. Sha, F.-X. Xie, F. Huang, Y. Cao, Optical and electrical effects of gold nanoparticles in the active layer of polymer solar cells, J. Mater. Chem. 22 (2012) 1206.
[22] F.X. Xie, W.C.H. Choy, C.C.D. Wang, W.E.I. Sha, D.D.S. Fung, Improving the efficiency of polymer solar cells by incorporating gold nanoparticles into all polymer layers, Appl. Phys. Lett. 99 (2011) 153304.
[23] C.C. Chang, H.L. Wu, C.H. Kuo, M.H. Huang, Hydrothermal synthesis of monodispersed octahedral gold nanocrystals with five different size ranges and their self-assembled structures, Chem. Mater. 20 (2008) 7570–7574.
[24] D.H. Wang, D.Y. Kim, K.W. Choi, J.H. Seo, S.H. Im, J.H. Park, O.O. Park, A.J. Heeger, Enhancement of donor–acceptor polymer bulk heterojunction solar cell power conversion efficiencies by addition of Au nanoparticles, Angew. Chem. Int. Ed. 50 (2011) 5519.
[25] D.Y. Kim, S.H. Im, O.O. Park, Y.T. Lim, Evolution of gold nanoparticles through Catalan, Archimedean, and Platonic solids, CrystEngComm 12 (2010) 116.
[26] B.J. Wiley, S.H. Im, Z.Y. Li, J. McLellan, A. Siekkinen, Y. Xia, Maneuvering the surface plasmon resonance of silver nanostructures through shape-controlled synthesis, J. Phys. Chem. B 110 (2006) 15666.
[27] J.P. Kottmann, O.J.F. Martin, D. Smith, S. Schultz, Plasmon resonances of silver nanowires with a nonregular cross section, Phys. Rev. B 64 (2001) 235402.
[28] J.Y. Kim, J.H. Jung, D.E. Lee, J. Joo, Enhancement of electrical conductivity of poly(3,4-ethylenedioxythiophene)/poly(4-styrenesulfonate) by a change of solvents, Synth. Met. 126 (2002) 311.
[29] C.S. Lee, J.Y. Kim, D.E. Lee, Y.K. Koo, J. Joo, S. Han, Y.W. Beag, S.K. Koh, Organic based flexible speaker through enhanced conductivity of PEDOT/PSS with various solvents, Synth. Met. 135–136 (2003) 13.
[30] S. Jeong, Y. Kwon, B.D. Choi, H. Ade, Y.S. Han, Improved efficiency of bulk heterojunction poly(3-hexylthiophene):[6,6]-phenyl-C_{61}-butyric acid methyl ester photovoltaic devices using discotic liquid crystal additives, Appl. Phys. Lett. 96 (2010) 183305.
[31] Y. Zhang, P.W.M. Blom, Electron and hole transport in poly(fluorene-benzothiadiazole), Appl. Phys. Lett. 98 (2011) 143504.
[32] T.Y. Chu, O.K. Song, Hole mobility of N,N′-bis(naphthalene-1-yl)-N,N′-bis(phenyl) benzidine investigated by using space-charge-limited currents, Appl. Phys. Lett. 90 (2007) 203512.